A machine learning based computational approach for prediction of cation distribution in spinel crystal

Special Collection: Machine Learning Hits Molecular Simulations

Ying Fang ; Paul R. Ohodnicki ; Guofeng Wang ■



J. Chem. Phys. 158, 194102 (2023) https://doi.org/10.1063/5.0146056





CrossMark

Articles You May Be Interested In

Giant tunnel magnetoresistance in polycrystalline magnetic tunnel junctions with highly textured $MgAl_2O_4(001)$ based barriers

Appl. Phys. Lett. (January 2018)

Fabrication of MgAl₂O₄ tunnel barrier by radio frequency-sputtering method and magnetoresistance effect through it with Fe or Fe₄N ferromagnetic electrode

Journal of Applied Physics (January 2015)

Magneto-dielectric and Magneto-resistive in the mixed spinel - MgFe₂O₄

AIP Conference Proceedings (May 2017)





A machine learning based computational approach for prediction of cation distribution in spinel crystal

Cite as: J. Chem. Phys. 158, 194102 (2023); doi: 10.1063/5.0146056 Submitted: 9 February 2023 • Accepted: 2 May 2023 •







Published Online: 15 May 2023





AFFILIATIONS

Department of Mechanical Engineering and Materials Science, University of Pittsburgh, Pittsburgh, Pennsylvania 15261, USA

Note: This paper is part of the JCP Special Topic on Machine Learning Hits Molecular Simulations.

a) Author to whom correspondence should be addressed: guw8@pitt.edu

ABSTRACT

In this study, a machine learning based computational approach has been developed to investigate the cation distribution in spinel crystals. The computational approach integrates the construction of datasets consisting of the energies calculated from density functional theory, the training of machine learning models to derive the relationship between system energy and structural features, and atomistic Monte Carlo simulations to sample the thermodynamic equilibrium structures of spinel crystals. It is found that the support vector machine model yields excellent performance in energy predictions based on spinel crystal structures. Furthermore, the developed computational approach has been applied to predict the cation distribution in single spinel MgAl₂O₄ and MgFe₂O₄ and double spinel MgAl_{2-a}Fe_aO₄. Agreeing with the available experimental data, the computational approach correctly predicts that the equilibrium degree of inversion of MgAl₂O₄ increases with temperature, whereas the degree of inversion of MgFe₂O₄ decreases with temperature. Additionally, it is predicted that the equilibrium occupancy of Mg cations at the tetrahedral and octahedral sites in MgAl_{2-a}Fe_aO₄ could be tuned as a function of chemical composition. Therefore, this study presents a reliable computational approach that can be extended to study the variation of cation distribution with processing temperature and chemical composition in a wide range of complex multi-cation spinel oxides with numerous applications.

Published under an exclusive license by AIP Publishing. https://doi.org/10.1063/5.0146056

I. INTRODUCTION

Metal oxides with spinel crystal structures have excellent and highly tunable mechanical, optical, magnetic, and electrical properties^{1,2} and, hence, broad applications, such as ferrofluids,³ wastewater treatment,4 biomedical devices,5 catalysts,6 gas sensors,7 electrodes,8 and inductive applications for electric power conversion and microwave technologies. A single spinel oxide has the formula of AB2O4, with A and B denoting metal cations and O denoting oxygen ions. The structure of a single spinel oxide can be viewed in a superlattice containing eight face-centered cubic unit cells and thirty-two O ions at the lattice points. In addition, eight tetrahedral sites and sixteen octahedral sites of the lattice are occupied by A and B cations. Figure 1(a) shows a normal spinel structure in which eight A cations occupy the tetrahedral sites and sixteen B cations occupy the octahedral sites. By contrast, Fig. 1(b) shows an inverse spinel structure in which eight B cations occupy the tetrahedral sites,

whereas the other eight B cations and eight A cations occupy the octahedral sites, respectively. The degree of inversion of an AB₂O₄ spinel crystal is, thus, defined as the fraction of the tetrahedral sites occupied by B cations and varies from a value of 0.0 in a normal structure to 1.0 in an inverse structure.

A solid solution of two single spinel oxides (especially a hybrid of the normal and inverse single spinels) forms a double spinel, ¹⁰ which has three different types of cations distributed at the tetrahedral and octahedral sites. Figure 1(c) shows a possible configuration of a double spinel. It has been found that the double spinel could exhibit superior performance as compared to the constituent single spinel in some applications, such as high-performance catalysts and coating materials against corrosion. 11-13 Zhou et al. synthesized double spinel ZnFe_{0.4}Co_{1.6}O₄, which shows a higher catalytic activity for the oxygen evolution reaction than its constituent single spinels ZnFe₂O₄ and ZnCo₂O₄. ¹¹ Joshi and Petric showed that double spinel Cu_{0.6}Ni_{0.4}Mn₂O₄ maintained an isothermal conductivity

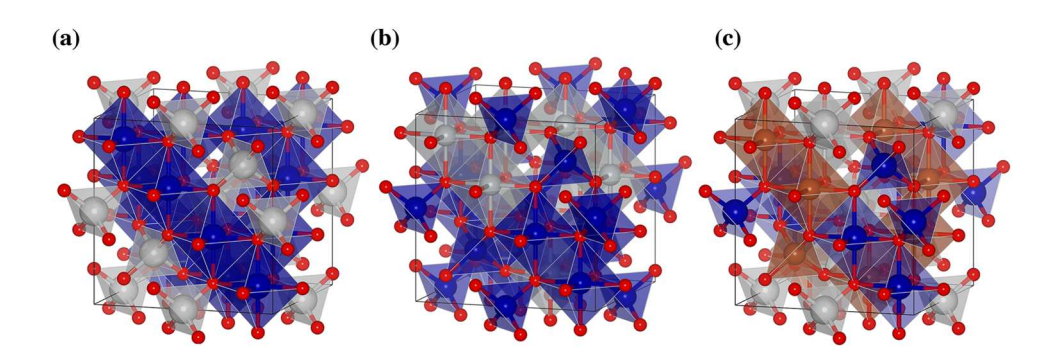


FIG. 1. Atomistic structure of (a) a normal structure of single spinel AB_2O_4 , (b) an inverse structure of single spinel AB_2O_4 , and (c) a double spinel crystal with composition $A(BC)O_4$. The red, gray, blue, and brown balls represent O ions, A cations, B cations, and C cations, respectively. The tetrahedrons and octahedrons enclose the tetrahedral and octahedral sites occupied by metal cations, respectively.

of ~70 S/cm at $600\,^{\circ}$ C, which is greater than that of $CuMn_2O_4$ and $NiMn_2O_4$. ¹² Moreover, Yadav *et al.* found that increasing the Nd content in double spinel $CoFe_{2-a}Nd_aO_4$ could enhance the total magnetization of the crystal. ¹³ It is widely believed that the modification of cation distribution in these double spinels as compared to those in the constituent single spinels is responsible for the observed property improvement. ^{11–13}

Many efforts have been devoted to the development of computational methods to accurately predict the cation distribution in single and double spinel oxides. 14-16 In this aspect, O'Neill et al. proposed a regular solution based thermodynamic model with consideration of electronic exchange reactions and size mismatch effects to predict the cation distribution and thermodynamic properties of double spinels.¹⁴ Most predictions from this model were found to agree with the experimental observation. However, the input parameters of this model were largely extracted from empirical data and, hence, subject to experimental uncertainties due to factors such as rates of cation distribution reactions, rates of electron exchange, and non-stoichiometry.¹⁴ Applying atomistic Monte Carlo simulations to sample the equilibrium cation distribution, Palin and Harrison developed a pairwise Buckingham-form interatomic potential to calculate the system energy of double spinel MgAl₂O₄-FeAl₂O₄. The predicted site occupancies of Mg, Al, and Fe cations on the tetrahedral and octahedral sites were found to agree with the available experimental measurement results. It should be pointed out that the employed interatomic potentials were not uniquely defined even for the same material system and they had to develop and compare the results of three different sets of parameters for MgAl₂O₄-FeAl₂O₄. Moreover, Pilania et al. employed a cluster expansion based effective Hamiltonian approach combined with canonical Monte Carlo simulations to predict the cation distribution in the normal-inverse double spinel MgAlGaO4 as a function of temperature. 16 To find the optimal effective cluster interactions for the spinel system, they used a genetic algorithm to minimize the error between the cluster expansion-predicted and density functional theory (DFT)computed configuration energies of spinel with different cation distributions. The computational approach was demonstrated to be capable of predicting ordered ground state, finite temperature cation ordering, and temperature-dependent cation distribution in double spinel MgAlGaO₄.

Recently, it has been demonstrated that integration of machine learning techniques with atomistic simulations could accelerate the computational modeling of material properties and behaviors. ^{17,18} For example, Yin *et al.* developed a machine-learning interatomic

potential for the refractory high entropy alloy MoNbTaW and, thus, enabled extensive molecular dynamics simulation of the motion of both edge and screw dislocations in the alloy over a wide range of temperatures.¹⁷ Yang *et al.* trained a neural network model over a DFT calculated dataset to evaluate the potential energy of CuPdAu surface slabs and further combined it with the Monte Carlo simulations to successfully predict the segregation profiles of the ternary alloys with varying overall compositions.¹⁸

Herein, we developed a DFT data-informed, machine-learning approach to evaluate the configurational energy of spinel and further employed atomistic Monte Carlo simulations to sample the thermodynamically equilibrium structures and cation distribution of spinel crystals at a given temperature. In order to validate the machine learning enabled atomistic simulation method, we applied it to predict the equilibrium temperature-dependent degree of inversion of single spinel MgAl $_2$ O $_4$ and MgFe $_2$ O $_4$, as well as the variation of cation distribution with chemical composition in double spinel MgAl $_2$ -aFe $_a$ O $_4$. The computational predictions are found to agree quite well with the experimental data from the literature. Consequently, machine learning techniques are demonstrated to be effective in accurately predicting the cation distribution in complex spinel oxides.

II. COMPUTATIONAL METHODS

A. Density functional theory (DFT) calculations

The first-principles spin-polarized calculations were performed using the Vienna Ab initio Simulation Package (VASP). 19 A plane wave basis associated with the projector-augmented wave approach was employed.²⁰ An exchange correlation was treated with generalized gradient approximation (GGA) in the form of the Perdew-Burke-Ernzerhof (PBE) functional.²¹ In all calculations, the plane-wave cutoff energy was set at 500 eV and the total energy of the system was converged within 10^{-6} eV. As in GGA+U calculations, the effective on-site Coulomb interaction parameter Ueff was chosen to be 4.0 eV on Fe ions. The structural optimization calculations used a 4 × 4 × 4 Monkhorst-Pack k-point mesh.²² Each structure was relaxed until the force on each atom was below 0.01 eV/Å. The special quasi-random structure (SQS) method implemented in Alloy Theoretic Automated Toolkit (ATAT) was used to construct the crystal structures that mimic the cation distribution in a random oxide.²³ In accordance with prior experimental results,²⁴ the ground state magnetic ordering in MgFe₂O₄ and MgAl_{2-a}Fe_aO₄ was set to

be that all the cations at the octahedral sites are of majority spin, whereas all the cations at the tetrahedral sites are of minority spin.

B. Monte Carlo simulation

The Monte Carlo (MC) simulation method based on the Metropolis algorithm was implemented to predict the cation distribution in spinel MgAl₂O₄, MgFe₂O₄, and MgAl_{2-a}Fe_aO₄ under thermodynamic equilibrium conditions. Starting from a given initial structure, we attempted to swap the positions of two randomly selected cations at each MC iteration. The energy associated with the structural change was calculated with the machine learning models. A Boltzmann distribution-based probability (p) was used to determine the acceptance or rejection of the attempted structural change. Specifically, probability $p = \min \left[1, \exp \left(-\frac{\Delta E}{k_B T} \right) \right]$, where ΔE is the energy caused by the structural change, k_B is the Boltzmann constant, and T is the system temperature. The equilibrium degree of inversion of spinel MgAl₂O₄ and MgFe₂O₄ and site occupancies of Mg, Al, and Fe cations in MgAl2-aFeaO4 were evaluated as the value averaged over 500 equilibrium structures sampled every 100 MC iterations during the last 50 000 iterations of the MC simulations.

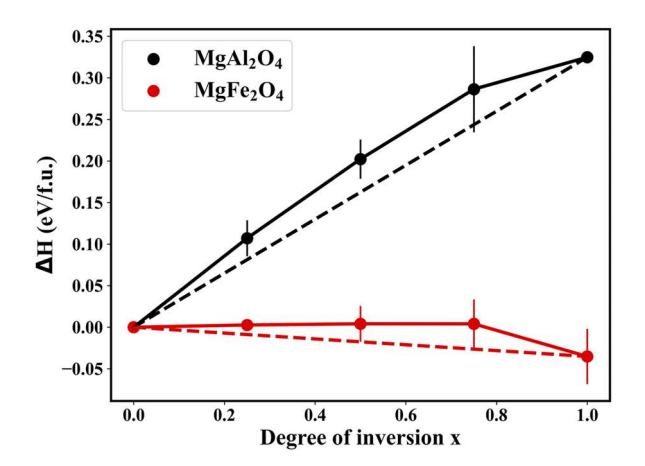
III. RESULTS AND DISCUSSION

A. Single spinel MgAl₂O₄ and MgFe₂O₄

1. Datasets

In this study, we first constructed datasets consisting of the energies and structures of single spinel crystals for training machine learning models. Included as the targeted property in the datasets, the system energies of single spinel MgAl₂O₄ and MgFe₂O₄ with various degrees of inversion have been calculated using the DFT method. The lattice parameter of MgAl₂O₄ in a normal spinel structure was predicted to be 8.17 Å, agreeing well with the previous computational value of 8.18 Å.25 The lattice parameter of MgFe₂O₄ with a degree of inversion of 0.75 was predicted to be 8.47 Å, consistent with the previous computational value of 8.52 Å and the experimental result of 8.40 Å. 26,27 Figure 2 plots the DFT calculated formation enthalpy (relative to the value of normal spinel structure) of single spinel MgAl₂O₄ and MgFe₂O₄ as a function of degree of inversion. The DFT results indicate that MgAl₂O₄ would prefer to have a normal spinel structure, whereas MgFe₂O₄ tends to have an inverse spinel structure at low temperatures. Moreover, noticeable deviations from the linear extrapolation (shown with the dashed lines) are indicative of interactions between cations on the allowed sublattices as mediated by the differences in various chemical bonds that arise as a result of the specific cation site occupation.²¹

Included as a structural feature in the datasets, the numbers of different types of cation–oxygen–cation bonds (denoted as M_1 –O– M_2), connecting two metal cations by an oxygen ion in single spinel MgAl₂O₄ and MgFe₂O₄, have been determined from crystal structure analysis. In our previous study,²⁸ we identified that the angles of the M_1 –O– M_2 bonds in a single spinel crystal had five possible values, namely 79°, 90°, 125°, 154°, and 180°, and there were two distinct types of M_1 –O– M_2 bonds with an angle of 125° owing to different bond lengths. Taking the permutation of distinct A and B cations into account, there should be 24 types of M_1 –O– M_2



 $\label{FIG. 2. Variation} FIG. 2. \ Variation of the DFT calculated formation enthalpy of single spinel MgAl_2O_4 and MgFe_2O_4 crystals as a function of degree of inversion. The error bars represent the standard deviation. The dashed lines show a linear extrapolation of the formation enthalpies of the normal and inverse spinel, analogous to an "ideal solid solution model" for chemical ordering on allowed sublattices.$

bonds in a single spinel crystal. However, the length of M₁-O is found to be equal to that of O-M2 only in the M1-O-M2 bond with an angle of 90°, causing bond A-O-B-90° to be the same as bond B-O-A-90°. Consequently, a single spinel crystal has a total of 23 distinct types of M₁-O-M₂ bonds. Thus, a twenty-threedimensional vector was used to describe each structure of single spinel MgAl₂O₄ and MgFe₂O₄ in our datasets. The values of the vector are the numbers of the represented type of the M₁-O-M₂ bonds in the crystal. It is worth pointing out that in the case of magnetic properties and magnetic spinel ferrites, the angle and distance of various M₁-O-M₂ bonds play an important role in determining the strength and sign of the super-exchange interaction between cations, thereby dictating properties such as magnetic ordering temperatures. Consequently, the present study paves the way for future studies to establish the relationship between magnetic properties and the structure of complex spinel oxides.

In Table I, we present the number of distinct spinel structures in the datasets for single spinel $MgAl_2O_4$ and $MgFe_2O_4$. Since $MgAl_2O_4$ is a prototypical normal spinel, more structures with a degree of inversion in the range from 0.25 to 0.75 are included. Because $MgFe_2O_4$ is predominantly an inverse spinel, more struc-

TABLE I. Numbers of distinct atomic structures of single spinel MgAl $_2$ O $_4$ and MgFe $_2$ O $_4$ with various degrees of inversion in the datasets for machine learning.

Degree of inversion (x)	$MgAl_2O_4$	MgFe ₂ O ₄
0.00	1	1
0.25	20	1
0.50	20	15
0.75	20	15
1.00	1	15
Total number	62	47

tures with a degree of inversion in the range from 0.50 to 1.00 are included in the datasets.

2. Machine learning

Four different machine learning models, namely linear regression, gradient booster machine, neural network, and support vector machine as implemented in scikit learn, 29,30 have been employed to find the relation between the system energy and structural features of single spinel MgAl₂O₄ and MgFe₂O₄. The linear regression by ordinary least squares assumes linearity between the structural features and the target property, whereas the other three machine learning models perform non-linear regression analysis. The gradient booster machine is a method to find a nonlinear relationship in the form of an ensemble of weak learners and further boost weak learners into a strong predictive model. The gradient booster machine has tunable hyperparameters, such as the maximum depth of individual regression estimators (max_depth), loss function, learning rate, and the number of boosting stages to perform (n_estimator).²⁹ The neural network consists of the input layer, hidden layers, and output layer, with a series of neurons in each layer. During the training process, each neuron in the hidden layers transforms the values from the previous layer by a weighted linear summation followed by a non-linear activation function. In the neural network model, the hyperparameters tuned include activation functions, hidden layer sizes, and the solver for weight optimization.²⁹ The support vector machine deals with non-linearity by transforming the input data into higher dimensions using kernel functions such as linear, polynomial (poly), and radial basis function (RBF). During the training of the support vector machine model, the types of kernel functions, the regularization parameter (C) associated with the training loss function, and the kernel coefficient (gamma) are tuned.2

Grid search and four-fold. cross-validation were used to find the optimal hyperparameters of the four machine learning models. During the fourfold cross-validation, 75% of the total data was used to train the machine learning models and the remaining 25% of the total data was used to test the performance of the predictions. In Table II, we give the hyperparameters of the three non-linear machine learning models optimized from the training set. The performance of the machine learning models was evaluated using metrics including mean absolute error (MAE), mean squared error (MSE), root mean squared error (RMSE), and the coefficient of determination (R²) between the predicted and DFT calculated data in the test set. The higher value of R² suggests a better fit of the model. With R² values ranging from 0.8331 to 0.9569 for

MgAl₂O₄ and 0.7971–0.9635 for MgFe₂O₄, all four models exhibit good performance in the prediction of the energies of the single spinel crystals.

Among the four machine learning models, the support vector machine was found to have the best performance in predicting the system energies of single spinel MgAl₂O₄ and MgFe₂O₄, as exhibited by the performance metrics in Table III. The support vector machine model for MgAl₂O₄, with a regularization parameter of 6.2 and a polynomial function as the kernel function, has an R² value of 0.9569 and an RMSE of 0.0121. For MgFe₂O₄, the support vector machine model uses the radial basis function as the kernel function and the regularization parameter of 2.3, producing energy predictions with an R² value of 0.9635 and an RMSE value of 0.0058. The success of the support vector machine model lies in its robustness in predicting nonlinear relationships and offering flexible hyperparameter tuning. In contrast, the linear regression was found to have the least predictive performance, with R² of 0.8331 and RMSE of 0.0171 for MgAl₂O₄ and R² of 0.7971 and RMSE of 0.0073 for MgFe₂O₄. Therefore, as compared to the linear regression, the support vector machine reduces the test set RMSE by 29.24% for MgAl₂O₄ and 20.55% for MgFe₂O₄, respectively. Such an improvement in predictive performance indicates that the nonlinearity between the system energy and the selected structural feature (i.e., the number of distinct types of M₁-O-M₂ bonds) of spinel crystal should be properly treated during machine learning. Figures 3(a) and 3(b) show the comparison between the best performing support vector machine model and DFT predicted energies for single spinel MgAl₂O₄ and MgFe₂O₄, respectively. It is noticeable that the data exhibit very slight scattering around the reference line, indicating the good predictive performance of the support vector machine model.

As plotted in Fig. 3(c), we have further examined the convergence of energy predictions from the support vector machine model with an increasing number of distinct structures in the datasets. At each given size, the specified numbers of data points were randomly selected from the whole dataset. For our analysis, such a random selection process of data had been repeated 100 times, and the fourfold cross-validation was performed each time. Hence, the value of RMSE at each given size of the dataset in Fig. 3(c) is the average value of 100 tests. The results in Fig. 3(c) show that RMSE converges well to the value for the whole dataset if the sub-datasets contain more than 50 distinct structures of MgAl₂O₄ and more than 30 distinct structures of MgFe₂O₄, respectively. Consequently, our whole datasets, as given in Table I, having 62 structures of MgAl₂O₄

TABLE II. Hyperparameters of machine learning models for single spinel MgAl₂O₄ and MgFe₂O₄.

	Model name	Selected parameters
MgAl ₂ O ₄	Gradient booster regression Neural network Support vector machine	max_depth = 5, loss function = square error, learning rate = 0.1, n_estimator = 4000 Activation function = logistic, hidden_layer_sizes = (20, 40), solver = lbfgs Kernel function = poly, C = 6.2, gamma = scale
MgFe ₂ O ₄	Gradient booster regression Neural network Support vector machine	max_depth = 7, loss function = square error, learning rate = 0.01, n_estimator = 7000 Activation function = logistic, hidden_layer_sizes = (120, 160), solver = lbfgs Kernel function = rbf, C = 2.3, gamma = scale

	Model name	MAE	MSE	RMSE	R ² value
	Linear regression	0.0137	0.0003	0.0171	0.8331
$MgAl_2O_4$	Gradient booster machine	0.0106	0.0003	0.0152	0.9342
	Neural network	0.0093	0.0002	0.0124	0.9525
	Support vector machine	0.0090	0.0002	0.0121	0.9569
	Linear regression	0.0050	0.00008	0.0073	0.7971
$MgFe_2O_4$	Gradient booster machine	0.0051	0.00005	0.0067	0.9429
	Neural network	0.0042	0.00005	0.0064	0.9440
	Support vector machine	0.0040	0.00004	0.0058	0.9635

TABLE III. Performance metrics of machine learning models for single spinel MgAl₂O₄ and MgFe₂O₄.

and 47 structures of MgFe $_2$ O $_4$, are sufficiently large and inclusive for the machine learning models to achieve acceptable accuracy of predictions.

3. Monte Carlo simulations

The well-trained linear regression model and support vector machine model were further applied in atomistic Monte Carlo simulations to predict the equilibrium cation distribution (i.e., degree of inversion) in single spinel MgAl $_2$ O $_4$ and MgFe $_2$ O $_4$. The simulation cells contain eight formula units of the spinel crystal and, thus, 56 atoms in total. For both spinel crystals, the initial structure was chosen to have a degree of inversion of 0.5 and the degree of inversion was allowed to evolve with the progression of the Monte Carlo simulations, which run in a total of 100 000 iterations at each given temperature. The temperature of the Monte Carlo simulations ranges from 473 to 1573 K. The equilibrium degree of inversion of MgAl $_2$ O $_4$ and MgFe $_2$ O $_4$ at a given temperature was thus evaluated by averaging the degree of inversion of 500 structures selected with a 100-step interval from the last 50 000 iterations of the Monte Carlo simulations.

Figure 4 shows the predicted degree of inversion of single spinel $MgAl_2O_4$ and $MgFe_2O_4$ as a function of temperature. Starting from

a value of 0.5, the degree of inversion of MgAl $_2$ O $_4$ decreases toward that of a normal spinel, whereas the degree of inversion of MgFe $_2$ O $_4$ increases toward that of an inverse spinel in the Monte Carlo simulations. Applying the support vector machine model in the Monte Carlo simulations, we predict quantitatively that the degree of inversion of MgAl $_2$ O $_4$ gradually increases with temperature from 0.009 at 676 K to 0.313 at 1573 K, whereas the degree of inversion of MgFe $_2$ O $_4$ decreases with temperature from 0.901 at 473 K to 0.736 at 1573 K. It is notable that our results agree well with previous experimental measurement results. $^{31-36}$

Furthermore, we conducted an analysis to quantify the errors in the DFT calculations and machine learning based computational approach as compared to experimental results in the literature. Table IV gives the formation energies of MgAl₂O₄ and MgFe₂O₄, both calculated from the DFT method³⁷ and measured experimentally, ^{38,39} showing an error of less than 1.4% in the DFT energy calculations. Using the machine learning based computational approach, the degree of inversion of MgAl₂O₄ at high temperature (1173 K) was predicted to be 0.191, very close to the value experimentally determined by Redfern *et al.* (x = 0.194 \pm 0.01)³¹ and Maekawa *et al.* (x = 0.211 \pm 0.015).³² At 1273 K, the degree of inversion of MgFe₂O₄ was predicted to be 0.740, which is also

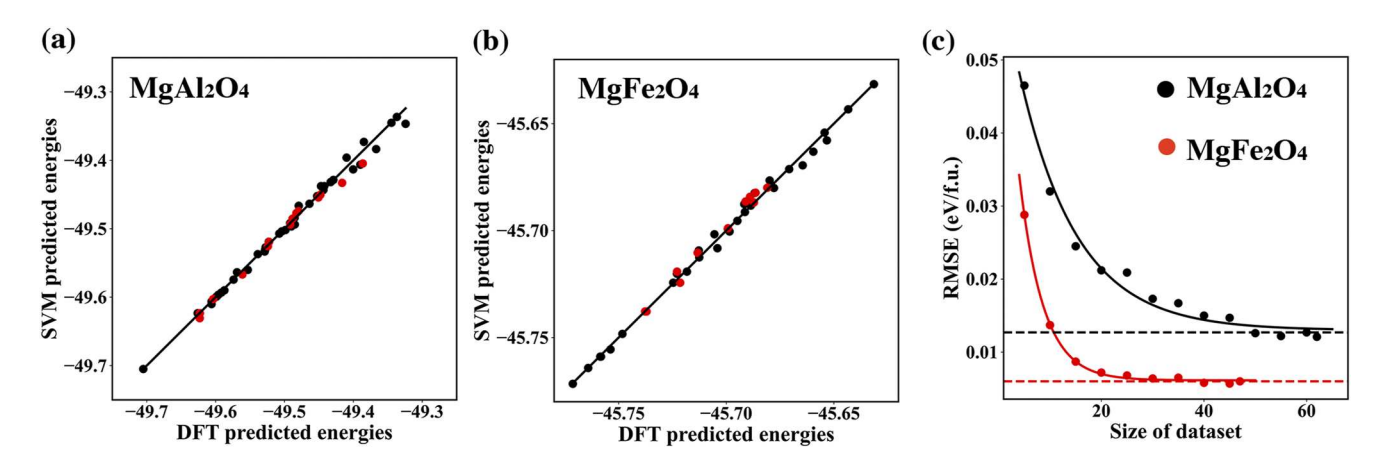


FIG. 3. DFT calculated energies as compared to the energies predicted from support vector machines for single spinel (a) MgAl₂O₄ and (b) MgFe₂O₄. In (a) and (b), the black and red dots show the data in the train dataset and test dataset, respectively. (c) Variation in the test set RMSE of the support vector machine model as a function of the number of different structures in the datasets for single spinel MgAl₂O₄ and MgFe₂O₄.

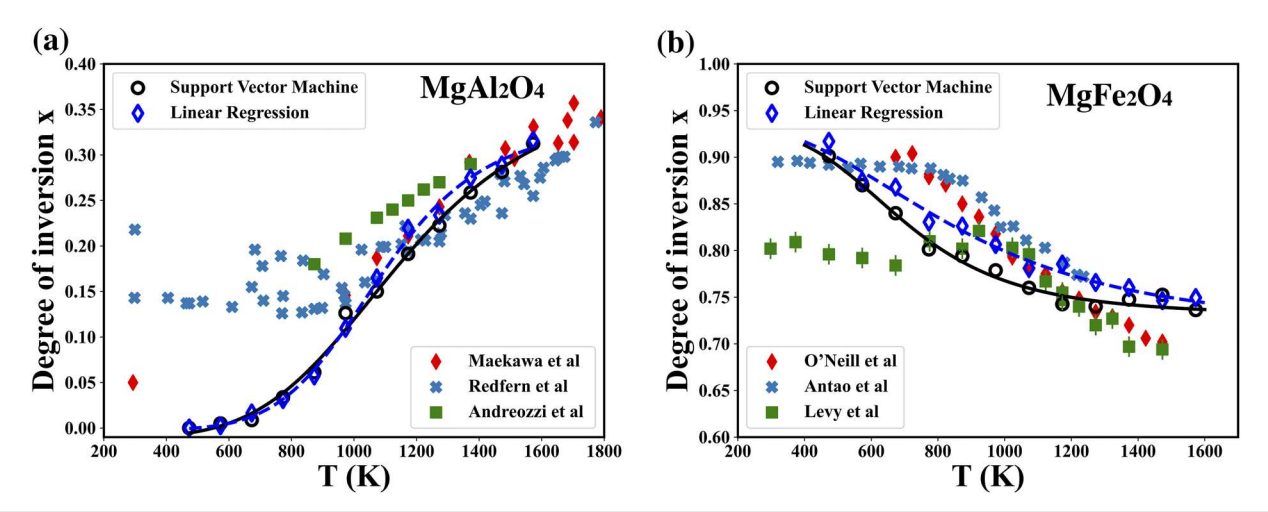


FIG. 4. Variation of degree of inversion of single spinel (a) MgAl₂O₄ and (b) MgFe₂O₄ as a function of temperature. Experimental data from Redfern *et al.*,³¹ Maekawa *et al.*,³² and Andreozzi *et al.*³⁵ for MgAl₂O₄ and from O'Neill *et al.*,³⁴ Antao *et al.*,³⁶ and Levy *et al.*³³ for MgFe₂O₄ are included for comparison with the machine learning model predictions.

TABLE IV. DFT predicted formation energies of single spinel $MgAl_2O_4$ (x=0.00) and $MgFe_2O_4$ (x=1.00) as compared to experimental values.

	DFT-PBE (eV/f.u.)	Experimental (eV/f.u.)	Error (%)
MgAl ₂ O ₄	-23.59	-23.80^{38}	0.9
$MgFe_2O_4$	-14.70	-14.91^{39}	1.4

very close to the values of 0.720 ± 0.011 measured by Levy *et al.*³³ and 0.734 ± 0.01 by O'Neill *et al.*³⁴ Consequently, the difference in the degree of inversion of a single spinel at a high temperature between the machine learning model predictions and experimental data was found to range from 0.003 to 0.02, which is in the same order of magnitude as the systematic error of experimental measurements. ^{31–34} However, Fig. 4(a) shows a much more pronounced discrepancy for the degree of inversion of MgAl₂O₄ at low temperatures between the machine learning model predictions and experimental data. This discrepancy might be attributed to the difficulty reaching thermal equilibrium states in experimental samples at low temperatures. Redfern *et al.* reported that the experimentally measured values of the degree of inversion could vary appreciably with different heat treatment processes at temperatures below 800 °C.³¹

Although the linear regression has an inferior predictive performance than the support vector machine, as shown in Table III, it is quite interesting to show in Fig. 4 that the two machine learning models give a pretty consistent prediction of the temperature-dependent degree of inversion of single spinel MgAl₂O₄ and MgFe₂O₄. It is noticeable that, for MgFe₂O₄, the predicted degree of inversion with the linear regression model is slightly higher than that with the support vector machine model in the temperature range studied. Therefore, our results demonstrate that the Monte Carlo simulations enabled by the support vector machine model can accurately predict the cation distribution (i.e., degree of inversion) in

single spinel MgAl₂O₄ and MgFe₂O₄, as validated by the available experimental results in Fig. 4.

B. Double spinel MgAl_{2-a}Fe_aO₄

1. Datasets

Furthermore, we extended the developed machine learning based computational approach to predict the cation distribution in double spinel MgAl_{2-a}Fe_aO₄. To this end, we added the DFT calculated system energies of the double spinel with various chemical compositions and cation distributions into the dataset. Table V presents the DFT predicted lattice parameters of the MgAl_{2-a}Fe_aO₄ crystal. The predicted lattice parameters agree well with the experimental results. 40 Moreover, our results show that the lattice parameter increases linearly with increasing content of Fe cations (denoted by *a*), due to the replacement of small Al cations with large Fe cations. 41

TABLE V. Predicted lattice parameters of double spinel MgAl_{2-a}Fe_aO₄ with various compositions and with a random cation distribution.

Composition (a) in MgAl _{2-a} Fe _a O ₄	Lattice parameter (Å)			
composition (w) in right 12-at va eq	This work	Experimental ⁴⁰		
0.00	8.17	8.09		
0.25	8.21	8.12		
0.50	8.25	8.16		
1.00	8.33			
1.25	8.36	8.28		
1.50	8.39	8.33		
1.75	8.43	8.34		
2.00	8.47	8.36		

TABLE VI. Summary of distinct structures in our dataset for double spinel MgAl_{2-a}Fe_aO₄. The crystal structure of double spinel consists of eight formula units and twenty-four metal cations.

Composition of Fe	Te	Tetrahedral site			ctahedral	Number	
in $MgAl_{2-a}Fe_aO_4$	Mg	Al	Fe	Mg	Al	Fe	of structures
	6	1	1	2	13	1	4
- 0.25	5	2	1	3	12	1	4
a = 0.25	4	3	1	4	11	1	4
	3	4	1	5	10	1	4
	6	1	1	2	11	3	4
a = 0.50	5	1	2	3	11	2	4
	4	2	2	4	10	2	4
	8	0	0	0	8	8	4
a = 1.00	6	1	1	2	7	7	4
	5	2	1	3	6	7	4
	3	1	4	5	5	12	4
a = 1.25	2	2	4	6	4	11	4
	2	1	5	6	5	11	4
	6	1	1	2	3	11	4
a = 1.50	5	1	2	3	3	10	4
	4	2	2	4	2	10	4
	2	0	6	6	2	8	4
a = 1.75	1	0	7	7	2	7	4
	1	1	6	7	1	8	4

As compared to single spinel, double spinel has the same configurations of $M_1\text{-}O\text{-}M_2$ bonds but has one additional type of cation. Based on the permutation of three distinct cations, there will be 51 different types of $M_1\text{-}O\text{-}M_2$ bonds in a double spinel crystal. Hence, a 51-dimensional vector was used to describe each structure of double spinel $MgAl_{2\text{-}a}Fe_aO_4$ and the values in the vector quantified the numbers of the represented types of the $M_1\text{-}O\text{-}M_2$ bonds in the crystal.

As shown in Table VI, we constructed a dataset specific for double spinel $MgAl_{2-a}Fe_aO_4$ with Fe content (a) varying from 0.25 to 1.75 and with different occupancies of Mg, Al, and Fe cations at the tetrahedral and octahedral sites. In total, our dataset contains the energies and structures of 76 distinct double spinel crystals.

2. Machine learning

For a comparative analysis, the four machine learning models have also been examined to derive the relationship between structural features and system energies of double spinel MgAl $_{2-a}$ Fe $_a$ O $_4$ using the dataset given in Table VI. Using the optimized parameters (Table VII), the four machine learning models consistently generate excellent energy predictions with an R 2 value above 0.99. As presented in Table VIII, the support vector machine model exhibits the best performance with an RSME value of 0.0161 and an R 2 value of 0.99974 by choosing a polynomial function as the kernel function and a regularization parameter of 7.0. The comparison between the DFT calculated energy and the predicted energy by the best performing support vector machine model is presented in Fig. 5(a).

TABLE VII. Hyperparameters of machine learning models for double spinel MgAl_{2-a}Fe_aO₄.

Model name	Selected parameters
Gradient booster machine Neural network Support vector machine	$max_depth = 100, loss function = square error, learning rate = 0.1, and n_estimator = 1500 \\ Activation function = identity, hidden_layer_sizes = (100, 200), and solver = lbfgs \\ Kernel function = poly, C = 7.0, and gamma = scale$

TABLE VIII. Performance metrics of machine learning models for double spinel ${\rm MgAl}_{2-a}{\rm Fe}_a{\rm O}_4$.

Model name	MAE	MSE	RMSE	R ² value
Linear regression	0.0130	0.0003	0.0174	0.99971
Gradient booster machine	0.0315	0.0017	0.0403	0.99849
Neural network	0.0130	0.0003	0.0173	0.99971
Support vector machine	0.0123	0.0003	0.0161	0.99974

A remarkably small scattering of the energies predicted from the support vector machine model with respect to those DFT-predicted energies was observed.

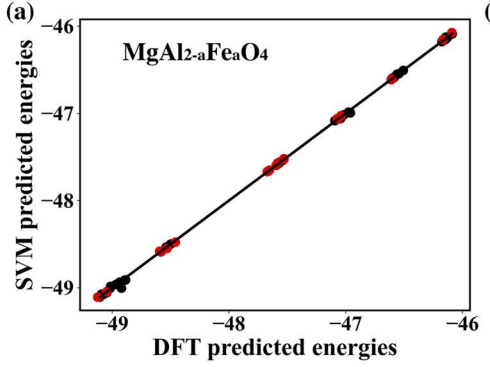
The convergence of energy predictions from the support vector machine model with an increasing number of distinct structures in the dataset of double spinel $\rm MgAl_{2-a}Fe_aO_4$ is plotted in Fig. 5(b). Our results show that the value of the test set RMSE is reduced by 85.63% when the number of distinct structures in the dataset increases from 10 to 76. The value of the test set RMSE for the dataset with 65 structures has already been very close to the value for the whole dataset of 76 structures. Therefore, our dataset for double spinel $\rm MgAl_{2-a}Fe_aO_4$ is sufficiently large and inclusive for the machine learning models to achieve acceptable accuracy in their predictions.

3. Monte Carlo simulations

In this study, we have compiled a dataset for the MgAl₂O₄-MgFe₂O₄ system, which includes 62 structures for single spinel MgAl₂O₄, 47 structures for single spinel MgFe₂O₄, and 76 structures for double spinel MgAl_{2-a}Fe_aO₄. The support vector machine model was trained over this whole dataset. With a regularization parameter of 4.0 and a polynomial function as the kernel function, the support vector machine model could achieve an impressive performance on the test set in the four-fold. crossvalidation with metrics of an R² value of 0.9991, a MAE of 0.0122, a MSE of 0.0011, and a RMSE of 0.0334. This well-trained support vector machine model was further applied in the atomistic Monte Carlo simulations to predict the equilibrium cation distribution in double spinel MgAl_{2-a}Fe_aO₄ at 1473 K. For comparison, we also used the same dataset to fit the interaction coefficients of a cluster expansion method, which has a total of 11 interaction coefficients and includes up to four-body interaction terms. 42-45 The predictive performance of the physics-based cluster expansion method on the test set in the four-fold. cross-validation was determined to be an \mathbb{R}^2 value of 0.9996, a MAE of 0.0210, a MSE of 0.0010, and a RMSE of 0.0313, closely comparable with that of the support vector machine model.

In the Monte Carlo simulations, the simulation cell consists of eight formula units with 56 atoms, and each Monte Carlo simulation runs 100 000 iterations. The initial structure was chosen to be the one with the lowest energy and the same composition in the dataset. Figure 6 shows the site occupancies of Mg, Al, or Fe cation in MgAl_{2-a}Fe_aO₄ predicted from the Monte Carlo simulations. The site occupancy was calculated as the average number of a specified type of cation over the number of the same sites (tetrahedral or octahedral) in the spinel crystal. As shown in Figs. 6(a)-6(c), consistent with an increase in Fe content (i.e., a varies from 0.0 to 2.0) in MgAl_{2-a}Fe_aO₄, the site occupancies of the Al cation decrease monotonously at both the tetrahedral sites (from 0.23 to 0.00) and octahedral sites (from 0.89 to 0.00), whereas those of the Fe cation increase monotonously at the tetrahedral sites (from 0.00 to 0.73) and octahedral sites (from 0.00 to 0.63). More interestingly, the site occupancy of the Mg cation was found to decrease from 0.77 to 0.27 at the tetrahedral sites but increase from 0.11 to 0.37 at the octahedral sites with increasing Fe content (i.e., decreasing Al content). Our predictions are found to agree excellently with the experimental results for the double spinel samples synthesized at 1473 K.⁴⁰ Moreover, Figs. 6(a)-6(c) show that the predicted cation site occupancies from the machine learning based support vector machine model and material physics based cluster expansion method agree excellently, indicating that the machine learning models based on a structure feature described only by M_1 –O– M_2 bonds have the same predictive performance as the computational method considering many-body interactions for spinel crystal.

In Fig. 6(d), we compare the fractions of Mg cation at the tetrahedral and octahedral sites. The fraction of Mg cations is calculated as the average number of Mg cations at the sites (tetrahedral or octahedral) over the total number of Mg cations. It was found that the fraction of Mg cations at the tetrahedral sites would decrease almost linearly from 0.77 to 0.27 (i.e., a linear increase in the fraction of Mg cations at the octahedral sites from 0.23 to 0.73) with the increase in the Fe content in double spinel MgAl_{2-a}Fe_aO₄. When the *a* of the Fe content reaches a value of about 1.2, the Mg cations at the tetrahedral and octahedral sites have an equal fraction. Consequently,



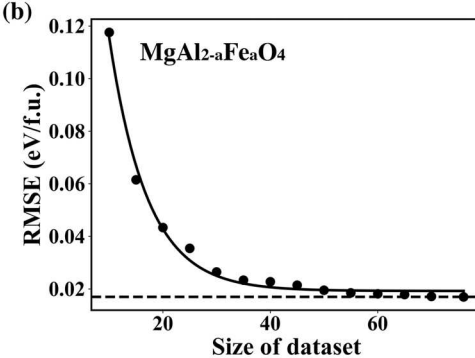


FIG. 5. (a) DFT calculated energies as compared to the energies predicted from the support vector machine for double spinel MgAl_{2-a}Fe_aO₄. In the figure, the black and red dots show the data in the train dataset and test dataset, respectively. (b) Variation in the test set RMSE of the support vector machine model as a function of the number of different structures in the dataset for double spinel MgAl_{2-a}Fe_aO₄.

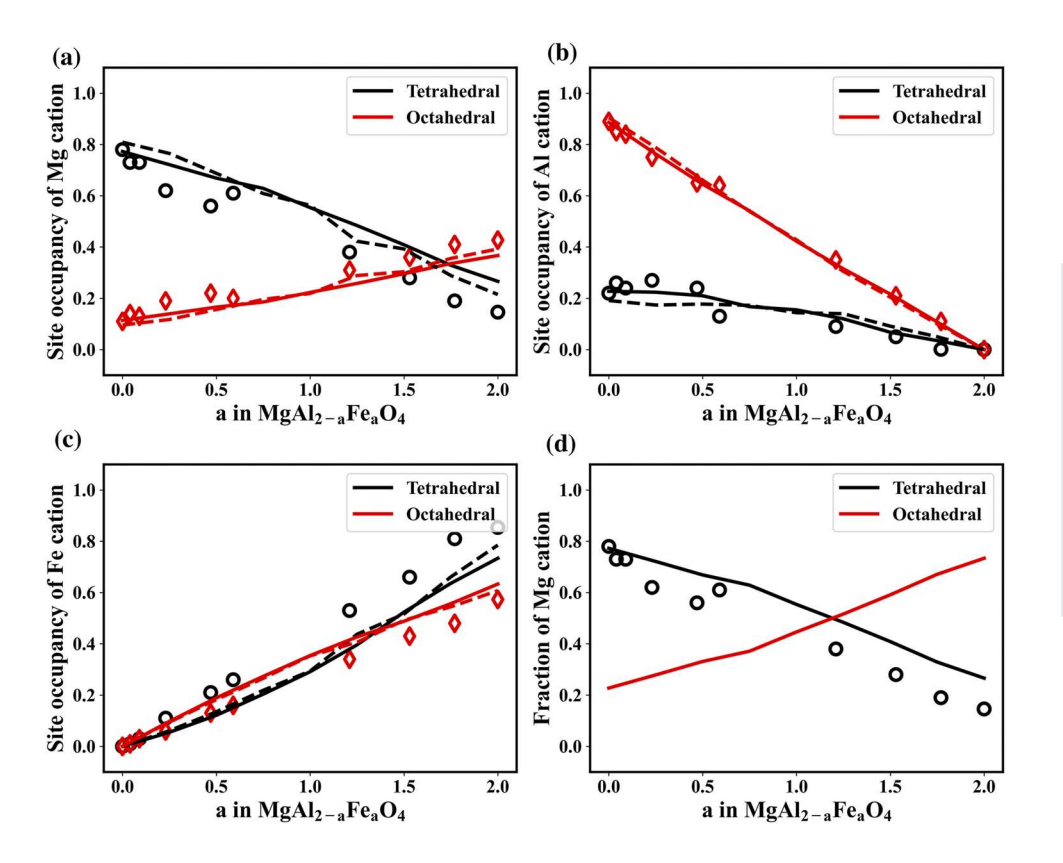


FIG. 6. Predicted site occupancy of (a) Mg, (b) Al, and (c) Fe cations as a function of Fe content in double spinel MgAl_{2-a}Fe_aO₄. The circles and diamonds show the experimentally measured site occupancies of the three cations at the tetrahedral and octahedral sites, respectively.⁴⁰ The dashed lines show the predictions with a cluster expansion method. (d) Predicted fraction of Mg cations occupied the tetrahedral and octahedral sites in double spinel MgAl_{2-a}Fe_aO₄. The circles represent the experimental results.⁴⁰

our results suggest that the fraction of Mg cations at different sites could be tuned by controlling the Fe and Al contents in double spinel $MgAl_{2}$. Fe Ω_{3}

It is worth mentioning that site occupation plays an important role in the overall magnetization of spinel crystal due to the cancellation of moments between two antiferromagnetically coupled sublattices.⁴⁶ Conventional models apply relatively simple factors, such as ionic valence, cation size, and crystal field as a function of chemistry, to predict the site preference energies of different cations in spinel crystals. Comparing these site preference energies,46 the tendency to occupy an octahedral site by Mg2+ was believed to be stronger than that of Fe³⁺ but less than that of Al³⁺. Hence, the conventional models qualitatively explain the preference of Mg cations at the octahedral sites in the inverse structure of MgFe₂O₄, the preference of Mg at the tetrahedral sites in the normal structure of MgAl₂O₄, and the variation of Mg site occupancy from the tetrahedral to octahedral sites with increasing Fe content in double spinel MgAl_{2-a}Fe_aO₄. In contrast, the current computational approach provides a much more quantitatively robust prediction of the site occupancy of cations with consideration of the plethora of bond types that occur, in practice, for complex multi-cation spinel ferrite systems.

IV. CONCLUSION

In this study, we constructed datasets consisting of the system energies and structural features of a wide variety of single

spinel MgAl $_2$ O $_4$ and MgFe $_2$ O $_4$ and double spinel MgAl $_2$ - $_a$ Fe $_a$ O $_4$ with different cation distributions. The system energies of these spinel oxides were computed using the DFT method. The structural features of these spinel oxides were represented using high-dimensional vectors containing the number of distinct types of M $_1$ -O-M $_2$ bonds in the crystal. Single spinel MgAl $_2$ O $_4$ and MgFe $_2$ O $_4$ have 23 distinct types of M $_1$ -O-M $_2$ bonds, whereas double spinel MgAl $_2$ - $_a$ Fe $_a$ O $_4$ has 51 distinct types of M $_1$ -O-M $_2$ bonds.

Four machine learning models, including linear regression, gradient booster machine, neural network, and support vector machine, have been examined to derive the relationship between the system energy and structural features of these spinel oxides. The performance of the machine learning models was evaluated using the metrics including MAE, MSE, RMSE, and R^2 on the test dataset. Among the four models, it was found that the support vector machine model led to the lowest RMSE and the highest R^2 in predicting the energies of single spinel MgAl $_2$ O $_4$ and MgFe $_2$ O $_4$ and double spinel MgAl $_2$ -aFe $_a$ O $_4$. The values of R^2 of the support vector machine model were calculated to be 0.9569 for MgAl $_2$ O $_4$, 0.9635 for MgFe $_2$ O $_4$, and 0.99974 for MgAl $_2$ -aFe $_a$ O $_4$, manifesting the high reliability of the derived structure–energy relation from this machine learning model.

Furthermore, the structure–energy relation derived from the support vector machine model was applied in atomistic Monte Carlo simulations to predict the equilibrium cation distribution in single spinel MgAl $_2$ O $_4$ and MgFe $_2$ O $_4$ and double spinel MgAl $_2$ -aFe $_a$ O $_4$. Simulation results show that MgAl $_2$ O $_4$ has an equilibrium crystal

structure close to the normal spinel crystal, but MgFe₂O₄ has a structure close to the inverse spinel crystal. Moreover, the degree of inversion of MgAl₂O₄ was predicted to increase with temperature from 0.009 at 676 K to 0.313 at 1573 K, whereas the degree of inversion of MgFe₂O₄ was found to decrease with temperature from 0.901 at 473 K to 0.736 at 1573 K. The predicted temperature-dependent degree of inversion of the two single spinel oxides is found to agree well with experimental data. For double spinel MgAl2-aFeaO4, the Monte Carlo simulation method was employed to predict the variation in the site occupancies of Mg, Al, and Fe cations with increasing Fe content. The simulation results indicated that the distribution of Mg cations at the tetrahedral and octahedral sites in double spinel MgAl_{2-a}Fe_aO₄ was tunable through the control of chemical composition. It was predicted that the fraction of Mg cations occupying the tetrahedral sites would decrease from 0.77 to 0.27 (i.e., increase from 0.23 to 0.73 at the octahedral sites) with a change of Fe content (i.e., a) from 0.0 to 2.0 in the double spinel. It should be noted that our computational results for the cation distribution in complex MgAl_{2-a}Fe_aO₄ agree quantitatively with experimental measurement results and are consistent with the qualitative predictions based on cation site preference energies.

Therefore, we have demonstrated that DFT data-informed, machine learning enabled Monte Carlo simulations could be used to predict the cation distribution in spinel crystals. The computational approach is well validated by the good agreement between the predicted and experimentally measured temperature-dependent degree of inversion of single spinel MgAl $_2$ O $_4$ and MgFe $_2$ O $_4$ and the variation of cation distribution with chemical composition in double spinel MgAl $_2$ - $_4$ Fe $_4$ O $_4$. The developed computational approach is expected to be a vital computational tool for future studies that aim to predict the cation distribution in complex spinel with multiple (i.e., four or five) types of metal cations.

ACKNOWLEDGMENTS

Wang acknowledges the support of the U.S. National Science Foundation (NSF DMR Grant No. 1905572 and NSF CMMI Grant No. 1760916). Ohodnicki acknowledges the support from the Office of Naval Research (ONR Grant No. 13330021). The authors also acknowledge the computational resources provided by the Center for Research Computing at the University of Pittsburgh.

AUTHOR DECLARATIONS

Conflict of Interest

The authors have no conflicts to disclose.

Author Contributions

Ying Fang: Data curation (equal); Formal analysis (equal); Investigation (equal); Methodology (equal); Validation (equal); Visualization (equal); Writing – original draft (equal). Paul R. Ohodnicki: Conceptualization (equal); Funding acquisition (equal); Project administration (equal); Resources (equal); Writing – review & editing (equal). Guofeng Wang: Conceptualization (equal); Funding acquisition (equal); Investigation (equal); Project administration

(equal); Resources (equal); Supervision (equal); Writing – review & editing (equal).

DATA AVAILABILITY

The data that support the findings of this study are openly available in GitHub at https://github.com/YIF27/Dataset-of-Spinel.

REFERENCES

- ¹ K. E. Sickafus, J. M. Wills, and N. W. Grimes, J. Am. Ceram. Soc. 82, 3279 (1999).
- ²L. Jaswal and B. Singh, J. Integr. Sci. Technol. **2**, 69 (2014) https://www.pubs.iscience.in/journal/index.php/jist/article/view/186.
- ³D. Makovec, A. Košak, A. Žnidaršič, and M. Drofenik, J. Magn. Magn. Mater. **289**, 32 (2005).
- ⁴J. R. Scheffe, J. Li, and A. W. Weimer, Int. J. Hydrogen Energy **35**, 3333 (2010).
- ⁵H. Chen, D. Billington, E. Riordan, J. Blomgren, S. R. Giblin, C. Johansson, and S. A. Majetich, Appl. Phys. Lett. **117**, 073702 (2020).
- ⁶S. Dey and G. C. Dhal, Mater. Sci. Energy Technol. 2, 575 (2019).
- ⁷ A. Šutka and K. A. Gross, Sens. Actuators, B **222**, 95 (2016).
- ⁸M. M. Thackeray, L. A. De Picciotto, A. De Kock, P. J. Johnson, V. A. Nicholas, and K. T. Adendorff, J. Power Sources 21, 1 (1987).
- ⁹ A. Goldman, *Modern Ferrite Technology* (Springer, New York, 2006).
- ¹⁰V. Kocevski, G. Pilania, and B. P. Uberuaga, J. Mater. Chem. A 8, 25756 (2020).
- ¹¹Y. Zhou, S. Sun, J. Song, S. Xi, B. Chen, Y. Du, A. C. Fisher, F. Cheng, X. Wang, H. Zhang, and Z. J. Xu, Adv. Mater. 30, 1802912 (2018).
- ¹²S. Joshi and A. Petric, Int. J. Hydrogen Energy **42**, 5584 (2017).
- ¹³R. S. Yadav, J. Havlica, J. Masilko, L. Kalina, J. Wasserbauer, M. Hajdúchová, V. Enev, I. Kuřitka, and Z. Kožáková, J. Magn. Magn. Mater. 399, 109 (2016).
- ¹⁴H. S. C. O'Neil and A. Navrotsky, Am. Mineral. 69, 733 (1984).
- ¹⁵E. J. Palin and R. J. Harrison, Mineral. Mag. **71**, 611 (2007).
- ¹⁶G. Pilania, V. Kocevski, J. A. Valdez, C. R. Kreller, and B. P. Uberuaga, Commun. Mater. 1, 84 (2020).
- ¹⁷S. Yin, Y. Zuo, A. Abu-Odeh, H. Zheng, X.-G. Li, J. Ding, S. P. Ong, M. Asta, and R. O. Ritchie, Nat. Commun. 12, 4873 (2021).
- ¹⁸Y. Yang, Z. Guo, A. J. Gellman, and J. R. Kitchin, J. Phys. Chem. C **126**, 1800 (2022).
- ¹⁹G. Kresse and J. Furthmüller, Phys. Rev. B **54**, 11169 (1996).
- ²⁰G. Kresse and D. Joubert, Phys. Rev. B **59**, 1758 (1999).
- ²¹ J. P. Perdew, K. Burke, and M. Ernzerhof, Phys. Rev. Lett. 77, 3865 (1996).
- ²²D. J. Chadi, Phys. Rev. B 16, 1746 (1977).
- ²³ A. Van de Walle, P. Tiwary, M. De Jong, D. L. Olmsted, M. Asta, A. Dick, D. Shin, Y. Wang, L.-Q. Chen, and Z.-K. Liu, Calphad 42, 13 (2013).
- ²⁴R. J. Harrison and A. Putnis, *Phys. Chem. Miner.* **26**, 322 (1999).
- ²⁵ J. A. Ball, M. Pirzada, R. W. Grimes, M. O. Zacate, D. W. Price, and B. P. Uberuaga, J. Phys.: Condens. Matter 17, 7621 (2005).
- ²⁶H. Guo, A. C. Marschilok, K. J. Takeuchi, E. S. Takeuchi, and P. Liu, Adv. Mater. Interfaces 6, 1901218 (2019).
- ²⁷W. C. Allen, J. Am. Ceram. Soc. **49**, 257 (1966).
- ²⁸Y. Fang, S. Zhang, P. R. Ohodnicki, and G. Wang, Mater. Today Commun. 33, 104436 (2022)
- ²⁹ F. Pedregosa, G. Varoquaux, A. Gramfort, V. Michel, B. Thirion, O. Grisel, M. Blondel, P. Prettenhofer, R. Weiss, V. Dubourg, J. Vanderplas, A. Passos, D. Cournapeau, M. Brucher, M. Perrot, and E. Duchesnay, J. Mach. Learn. Res. 12, 2825 (2011) arXiv:1201.0490 (2012).
- ³⁰G. Hackeling, Mastering Machine Learning with Scikit-Learn (Packt Publishing Ltd., Birmingham, 2017).
- ³¹S. A. T. Redfern, R. J. Harrison, H. S. C. O'Neill, and D. R. R. Wood, Am. Mineral. 84, 299 (1999).
- ³² H. Maekawa, S. Kato, K. Kawamura, and T. Yokokawa, Am. Mineral. 82, 1125 (1997).
- ³³D. Levy, V. Diella, M. Dapiaggi, A. Sani, M. Gemmi, and A. Pavese, Phys. Chem. Miner. 31, 122 (2004).

- ³⁴H. S. C. O'Neill, H. Annersten, and D. Virgo, Am. Mineral. 77, 725 (1992).
- ³⁵G. B. Andreozzi, F. Princivalle, H. Skogby, and A. Della Giusta, Am. Mineral. 85, 1164 (2000).
- ³⁶S. M. Antao, I. Hassan, and J. B. Parise, Am. Mineral. **90**, 219 (2005).
- ³⁷A. Wang, R. Kingsbury, M. McDermott, M. Horton, A. Jain, S. P. Ong, S. Dwaraknath, and K. A. Persson, Sci. Rep. 11, 15496 (2021).
- ³⁸P. J. Linstrom and W. G. Mallard ,J. Chem. *Eng. Data.* **46**, 1059 (2001).
- ³⁹V. M. Khot, A. B. Salunkhe, M. R. Phadatare, and S. H. Pawar, Mater. Chem. Phys. **132**, 782 (2012).
- ⁴⁰ A. Nakatsuka, H. Ueno, N. Nakayama, T. Mizota, and H. Maekawa, Phys. Chem. Miner. 31, 278 (2004).
- ⁴¹ K. B. Modi, H. H. Joshi, and R. G. Kulkarni, J. Mater. Sci. 31, 1311 (1996).
- ⁴²S. Hao, Z. Lu, and C. Wolverton, Phys. Rev. B **94**, 014114 (2016).
- ⁴³A. R. Natarajan and A. Van der Ven, npj Comput. Mater. **4**, 56 (2018).
- ⁴⁴L. Barroso-Luque, J. H. Yang, F. Xie, T. Chen, R. L. Kam, Z. Jadidi, P. Zhong, and G. Ceder, J. Open Source Software 7, 4504 (2022).
- ⁴⁵L. Barroso-Luque, P. Zhong, J. H. Yang, F. Xie, T. Chen, B. Ouyang, and G. Ceder, Phys. Rev. B 106, 144202 (2022).
- ⁴⁶R. C. O'Handley, *Modern Magnetic Materials: Principles and Applications* (Wiley, New York, 2000).